Kozumplik, Joanne (ASRC) 470802

From: STIC-EIC1700
Sent: Wednesday, October 29, 2003 9:06 AM
To: STIC-ILL
Subject: FW: 10038600

-----Original Message-----
From: Gakh, Yelena
Sent: Tuesday, October 28, 2003 5:49 PM
To: STIC-EIC1700
Subject: 10038600

Hi, Kendra,

please order the following:

7. TITLE: "Combinatorial methods for advanced materials research & development"
AUTHOR(S): *Cremer, R.; Dondorf, S.; Hauck, M.; Horbach, D.; Kaiser, M.; Kyrsta, S.; Kyrylov, O.; Munstermann, E.; Philipps, M.; Reichert, K.; Strauch, G.*
CORPORATE SOURCE: Rheinisch-Westfalische Technische Hochschule Aachen, Aachen, Germany
SOURCE: **Zeitschrift fuer Metallkunde (2001), 92(10), 1120-1127**

Thanks,

Yelena

Yelena G. Gakh, Ph.D.

Patent Examiner
USPTO, cp3/7B-08
(703)306-5906

R. Cremer, S. Dondorf, M. Hauck, D. Horbach, M. Kaiser, S. Kyrsta, O. Kyrylov, E. Münstermann, M. Philipps, K. Reichert, G. Strauch

Lehrstuhl für Theoretische Hüttenkunde, Rheinisch-Westfälische Technische Hochschule Aachen, Aachen, Germany

Combinatorial Methods for Advanced Materials Research & Development

Dedicated to Professor Dr.-Ing. Dieter Neuschütz on the occasion of his 65th birthday

The applicability of combinatorial methods in developing advanced materials is illustrated presenting four examples for the deposition and characterization of one- and two-dimensionally laterally graded coatings, which were deposited by means of (reactive) magnetron sputtering and plasma-enhanced chemical vapor deposition. To emphasize the advantages of combinatorial approaches, metastable hard coatings like (Ti,Al)N and (Ti,Al,Hf)N respectively, as well as Ge–Sb–Te based films for rewritable optical data storage were investigated with respect to the relations between structure, composition, and the desired materials properties.

Keywords: Combinatorial materials synthesis; Magnetron sputtering; Plasma-enhanced chemical vapor deposition; Metastable hard coatings; Phase change materials

Kombinatorische Methoden zur Entwicklung fortschrittlicher Werkstoffe

Die Anwendbarkeit kombinatorischer Methoden für die Entwicklung fortschrittlicher Werkstoffe wird an vier Beispielen zur Abscheidung und Charakterisierung ein- und zweidimensional gradierter Schichten verdeutlicht. Hierbei erfolgte die Abscheidung der Schichten sowohl mittels (reaktivem) Magnetronsputtern als auch mittels plasmaunterstützter chemischer Gasphasenabscheidung. Um die Vorteile kombinatorischer Ansätze herauszustellen, wurden anhand metastabiler Hartstoffschichten wie (Ti,Al)N bzw. (Ti,Al,Hf)N sowie Ge–Sb–Te-Schichten für wiederbeschreibbare optische Datenspeicher die Zusammenhänge zwischen Struktur, Zusammensetzung und gewünschten Materialeigenschaften, wie z. B. Oxidationsbeständigkeit, Härte oder Phasenumwandlungsgeschwindigkeit, untersucht.

1 Introduction

Looking at nature, the observer scarcely realizes that even the most beautiful and most complicated achievements of nature (Fig. 1) are the result of a persisting struggle between the competing species and that every progress in evolution is the result of a brutal algorithm based on mutation and selection. This interpretation of evolution, well known as "Darwin's theory" [59Dar], has proven its efficiency from the very first beginning to the complexity of modern life and is still an ongoing story of success. As in many scientific areas, materials scientists look with interest at this successful principle and try to adapt the technique of producing a large number of variations and a subsequent evaluation of this "library" to materials science.

First approaches to this so-called combinatorial science were made in the early '90s by the pharmaceutical industry and recently to the screening of superconductive, magnetoresistant, and photoluminescent materials [99Jan]. In contrast to the complex masking techniques and subsequent diffusion treatments, which are usually used in combinatorial materials development (Fig. 2) [99Jan], the composition-spread approach for materials development [69Saw, 98Dov, 01Kyr] is much less established. In this approach, two or three material sources (e.g. magnetron cathodes) are adjusted to the sample under a defined angle (Fig. 3), resulting in a film with a one- or two-dimensionally graded composition. In combination with an analytical technique with high lateral resolution, a fast examination of the process window of thin films or coatings is possible. This approach has originally been suggested by Hanak [70Han] three decades

Fig. 1. "There is grandeur in this view of life, with its several powers, having been originally breathed into a few forms or into one; and that, whilst this planet has gone cycling on according to the fixed law of gravity, from so simple a beginning endless forms most beautiful and most wonderful have been, and are being, evolved" [59Dar].

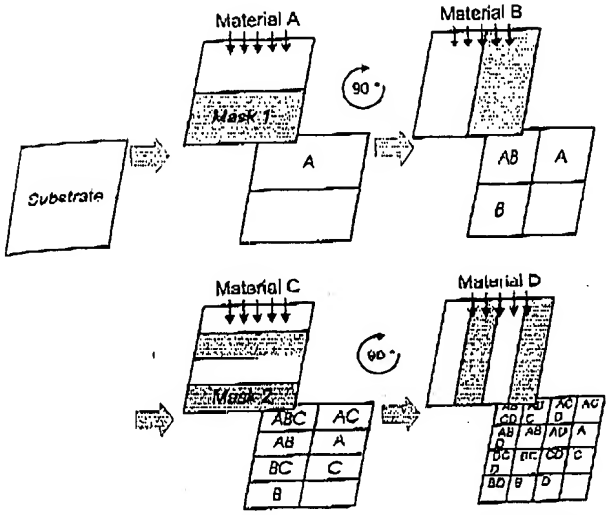

Fig. 2. Typical masking system for the deposition of a materials library.

ago and has been called "multiple-sample concept", but it took until the late '90s to incorporate his concept into modern combinatorial approaches to materials discovery

The present paper outlines the opportunities offered by the adaptation of combinatorial methods to advanced materials development. For this, four different investigations, all using combinatorial approaches transferred into both physical vapor deposition (PVD) and plasma-enhanced chemical vapor deposition (PECVD) (Fig. 4) techniques, are discussed.

2 Oxidation Resistance of One-Dimensionally Graded (Ti, Al) N ⇒ (Ti, Al) N PVD Coatings

2.1 Experimental

Metastable, single-phase, polycrystalline $Ti_{1-x}Al_xN$ hard coatings were deposited on HSS substrates by reactive magnetron sputtering. The substrate temperature was 100 °C, the applied bias was −40 V. The argon pressure was held at 0.36 Pa, the nitrogen reactive gas pressure at 0.11 Pa, and the total sputter power was 600 W DC. To produce coatings with a lateral gradient in composition, a dual cathode arrangement was used. The two cathodes, equipped with aluminum and titanium targets, respectively, were adjusted at a low angle to the surface. Additionally, a system of apertures was mounted between the cathodes (Fig. 3a).

Oxidation of the films was carried out in a high temperature SiC tube furnace. The oxidation conditions were: flowing synthetic air with $p(N_2) = 7.9 \times 10^4$ Pa and $p(O_2) = 2.1 \times 10^4$ Pa; oxidation temperature 815 °C; oxidation time 1 h. The composition of the as-deposited films as well as of the oxidized coatings was determined by electron probe microanalysis (EPMA) in a Camebax SX 50 microprobe.

2.2 Results and Discussion

The composition of the laterally graded coating as a function of the position on the substrate is given in Fig. 5. Obviously, neither the oxygen nor the nitrogen content is significantly dependent on the lateral position. The average nitrogen content of the coating is about 46 at.%, whereas the oxygen content is approximately 4 at.%. The titanium content of the coating decreases from about 28 to 5 at.%, correlated to a simultaneous increase of the aluminum content from about 20 to 44 at.%.

In Fig. 6, the total oxygen content of the oxidized coating is plotted as a function of the substrate composition at the

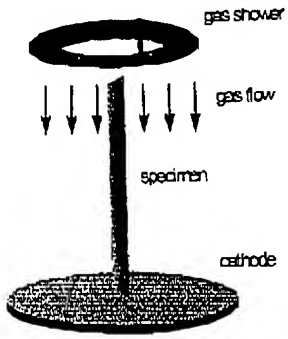

Fig. 4. Schematic illustration of substrate position and gas flow inside the PECVD reaction chamber.

corresponding point. Obviously, an almost linear correlation between the oxygen content and thus the thickness of the oxidic scale and the AlN content of the (Ti,Al)N coating can be observed. The scatter in the oxygen signal due to the formation of microcracks occurs at a composition of about $Ti_{0.25}Al_{0.75}N$. This observation is in accordance with previous investigations of the oxidation resistance of hexagonal (Ti,Al)N films [97Cre].

3 Structure of Two-Dimensionally Graded (Ti,Al,Hf)N PVD Hard Coatings

3.1 Experimental

A Ti–Al–Hf–N hard coating was deposited on a 2″ silicon wafer by reactive DC magnetron sputtering. Prior to the

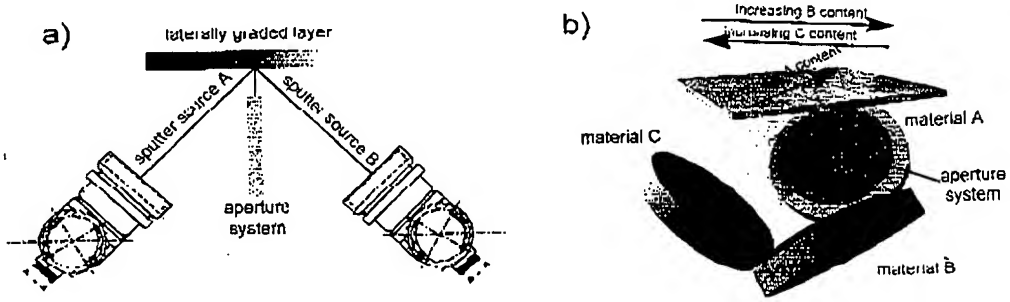

Fig. 3. Experimental set-up for one- and two-dimensional composition-spreads.

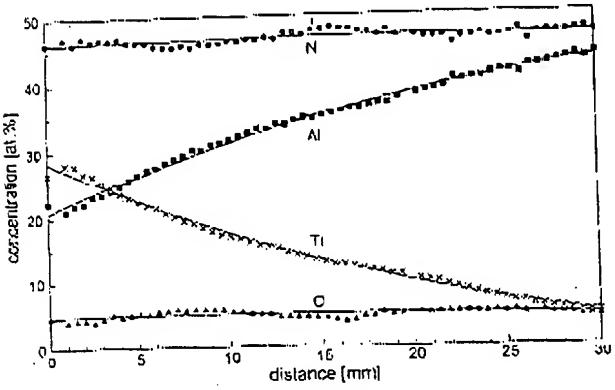

Fig. 5. Composition of the as-deposited (Ti,Al)N coating as a function of the position on the substrate.

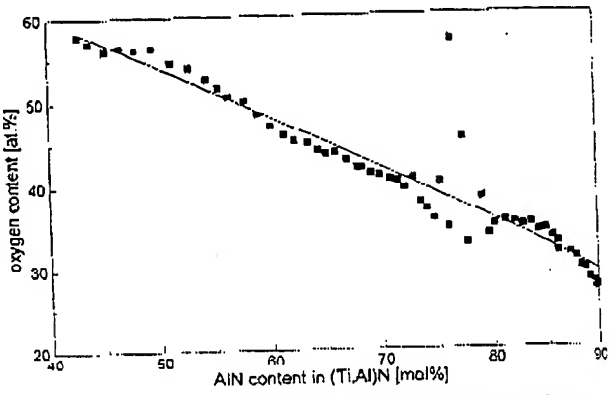

Fig. 6. Total oxygen content of the oxidized (Ti,Al)N coating as a function of substrate composition.

film deposition, a thin (d < 10 nm) Ti buffer layer was deposited. The substrate temperature was 200 °C, the applied bias −40 V, the Ar pressure 0.36 Pa, and the sputter power 300 W for each cathode. To enable a lateral compositional gradient in the coating, a triple cathode arrangement was used, i. e., adjusting the three cathodes, equipped with aluminum, titanium and hafnium targets, respectively, at a low angle to the surface. Additionally, a system of apertures was mounted between the cathodes (Fig. 3b). The nitrogen reactive gas pressure was 0.11 Pa

The composition of the as-deposited films was determined by EPMA. Structural analyses were performed in a Bruker AXS D8 system equipped with a general area detector diffraction system (GADDS) for fast structural mapping. Acquisition time was 120 s per spectrum, the angle of incidence of the X-ray source was held fixed at 10°, the incident beam spot size was adjusted to 500 µm. Spectra were recorded in the $25° < 2\Theta < 55°$ range. For structural analyses, a 7×7 array within a rectangle of 32×32 mm^2 was measured in the middle of the wafer (Fig. 7). The positions of the three individual cathodes with respect to the substrate position are inserted into the figure.

3.2 Results and Discussion

The composition of the laterally graded Ti−Al−Hf−N coating as a function of the position on the substrate is given in Fig. 8. The compositional mappings were determined in an area of 32×32 mm^2. Obviously, the nitrogen content of the coating does not significantly depend on the position on the substrate and varies between 50 and 54 at.%. The aluminum content decreases from top to bottom combined with a simultaneous increase in titanium content. The hafnium content of the coating decreases from left to right from values of about 14 at.% to zero.

The crystallographic structure of the films is given in Fig. 9. Four sections have been chosen to illustrate the influence of the composition on the crystallographic structure of the film.

In the bottom right part of Fig. 9, the effect of aluminum addition to the TiN lattice is demonstrated. With increasing Al content the lattice parameter of the face-centered cubic B1 ordered unit cell decreases due to the incorporation of smaller Al atoms into the lattice. In addition, the texture of the film changes significantly, resulting in a strong (200) texture at positions 4 and 5. A further increase of the Al content results in the formation of the hexagonal B4 structure of AlN and a concurrent change in texture of the cubic phase.

The effect of Hf additions into the cubic TiN structure is given in the bottom left figure. Due to the incorporation of larger hafnium atoms into the structure, the lattice parameter increases from right to left. Simultaneously the texture of the film changes from nearly untextured to a (200) texture and finally to a (111) texture.

In the upper part of the figure, the influence of slight Hf additions to the hexagonal AlN (right) and the effect of Al additions to the cubic structure of Hf-rich (Ti,Hf)N (left) are given. Obviously, Hf additions to the hexagonal B4 structure led not only to an increase of the lattice parameters, but also to a significant change in texture of the hexagonal phase, i. e., from distinctly (101)-textured to almost untextured. However, aluminum additions to the B1 ordered structure of Hf-rich (Ti,Hf)N led to an early formation of a two-phase mixture of cubic and hexagonal phases in position 3 and finally to the single-phase B4 ordered structure.

4 Microhardness of One-Dimensionally Graded (Ti, Al) N ⇒ (Ti, Al) N PECVD Coatings

4.1 Experimental

(Ti,Al)N films have been deposited on high-speed steel (HSS) by means of PECVD in a pulsed DC glow discharge

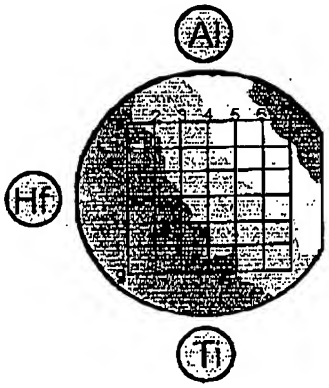

Fig. 7. Arrangement of the elemental and structural mapping on the Si wafer. Elemental mappings were carried out within a 32×32 mm^2 area. The structure of the coatings was determined in the same area using a 7×7 grid. The positions of the three individual cathodes with respect to the substrate position are inserted into the figure.

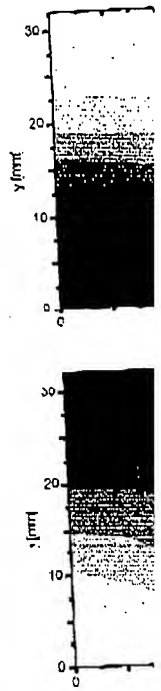

Fig. 8. Elemet

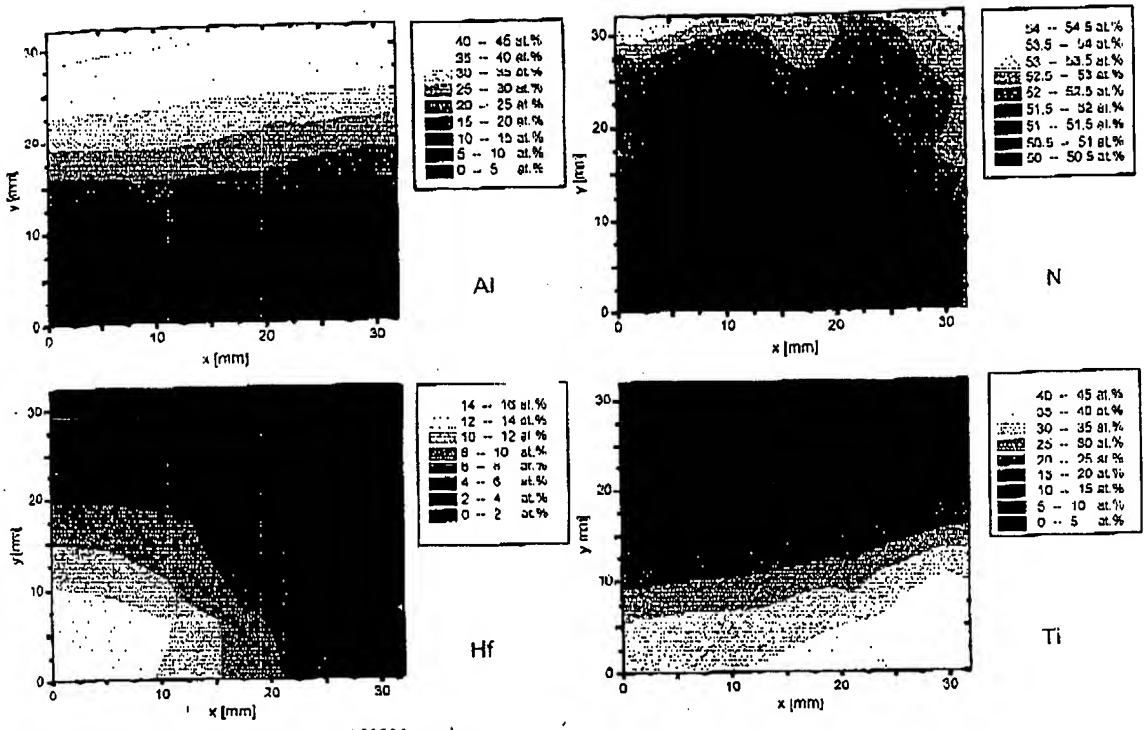

Fig. 8. Elemental mapping of the (Ti,Al,Hf)N coating.

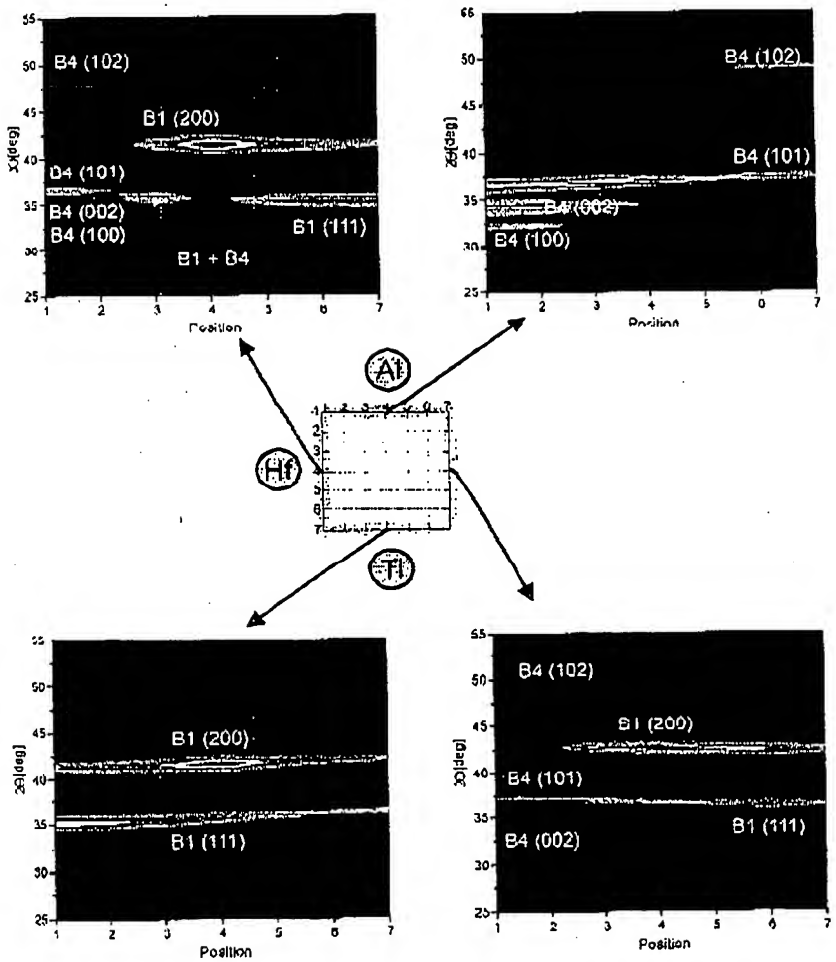

Fig. 9. Four sections of the structural mapping of the (Ti,Al,Hf)N coating. The relative positions of the three cathodes with respect to the substrate are also inserted into the figure.

Table 1. Deposition parameters for PECVD $(Ti_{1-x}Al_x)N$.

Total pressure	1.5 mbar
Substrate temperature	510 °C
Pulse time	50 µs
Pulse/pause ratio	0.5–2
Flow rate of $TiCl_4$	0.123 sl/h
Al/Ti input ratio	3
H/Cl input ratio	11
Ar concentration	14 %

Table 2. Chemical composition of the coatings deposited at 480 V discharge voltage.

Distance from gas inlet [mm]	Contents [at.%]			
	Ti	Al	N	Cl
43	30.6	17.4	48.2	3.8
98	14.4	34.2	48.5	2.9
151	2.9	59.7	35.8	1.6

from $TiCl_4-AlCl_3-H_2-N_2-Ar$ gaseous mixtures. The experimental set-up is described in detail elsewhere [99Pra]. $AlCl_3$ was generated in situ by the reaction of HCl with 99.99 % pure aluminum chips at a temperature of 500 °C. After grinding and polishing, the 15 cm long specimens were placed vertically in the middle of the cathode of the pulsed DC plasma source with the bell of the vacuum chamber acting as the anode. To obtain a good lateral gas distribution and yet a vertical gradient within the process chamber, a gas shower system was used (Fig. 4). The deposition parameters are listed in Table 1. The experiments were carried out at discharge voltages of 430, 480 and 530 V at a constant precursor flow rate.

The morphology and the chemical composition of the films were investigated by scanning electron microscopy (SEM) and energy-dispersive X-ray analysis (EDX), respectively. The crystallographic structure was determined by grazing incidence X-ray diffraction (GIXRD) in a Siemens D 500 goniometer using 900 W Cu Kα radiation.

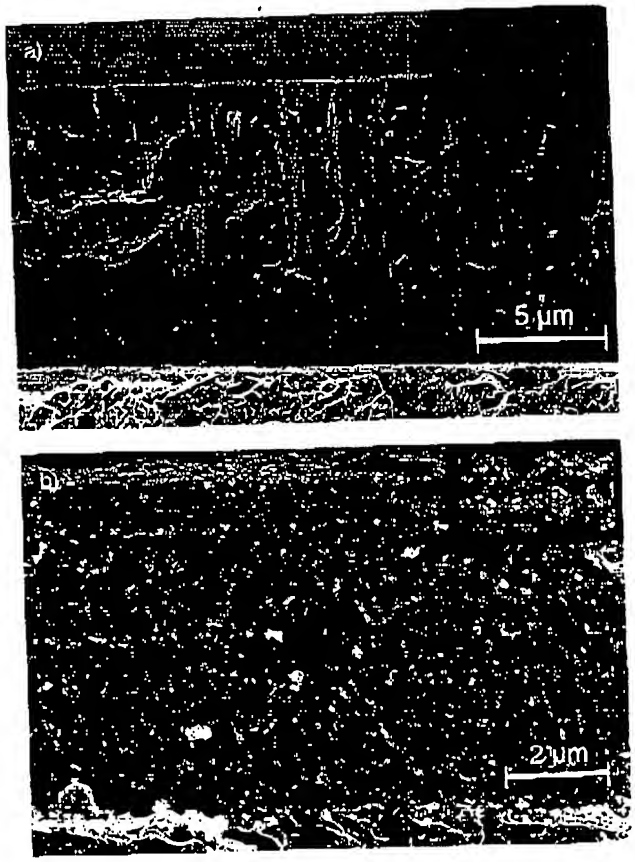

Fig. 11. Cross-sectional micrographs of the (Ti,Al)N film deposited at a distance of 41 mm (a) and 151 mm (b) from the gas inlet. The surface topography of the film, taken at the same magnification, is inserted in the upper right corner of the figures.

4.2 Results and Discussion

Due to the faster depletion of $TiCl_4$ within the gas phase as compared to $AlCl_3$, the experimental set-up leads to the deposition of metastable (Ti,Al)N films with a compositional gradient. To examine the change of the crystallographic structure, diffraction patterns of the coatings were taken at

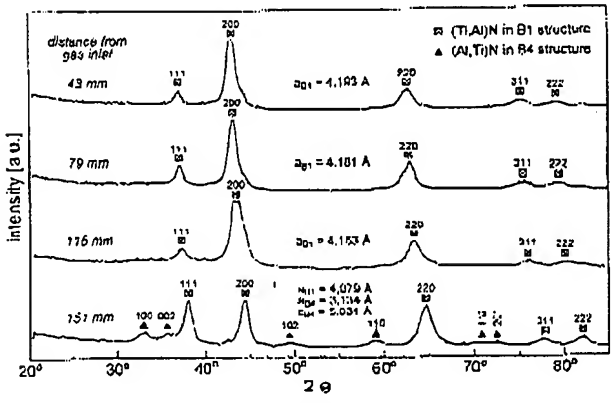

Fig. 10. GIXRD patterns of the (Ti,Al)N coating, deposited by PECVD at a discharge voltage of 480 V, at different distances from the gas inlet.

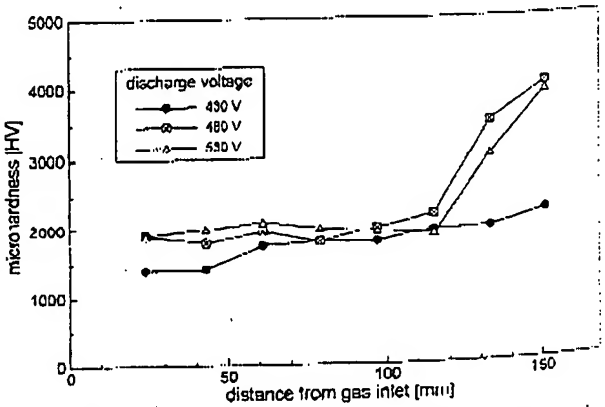

Fig. 12. Microhardness of (Ti, Al) N films, deposited at different discharge voltages, as a function of the substrate to gas inlet distance.

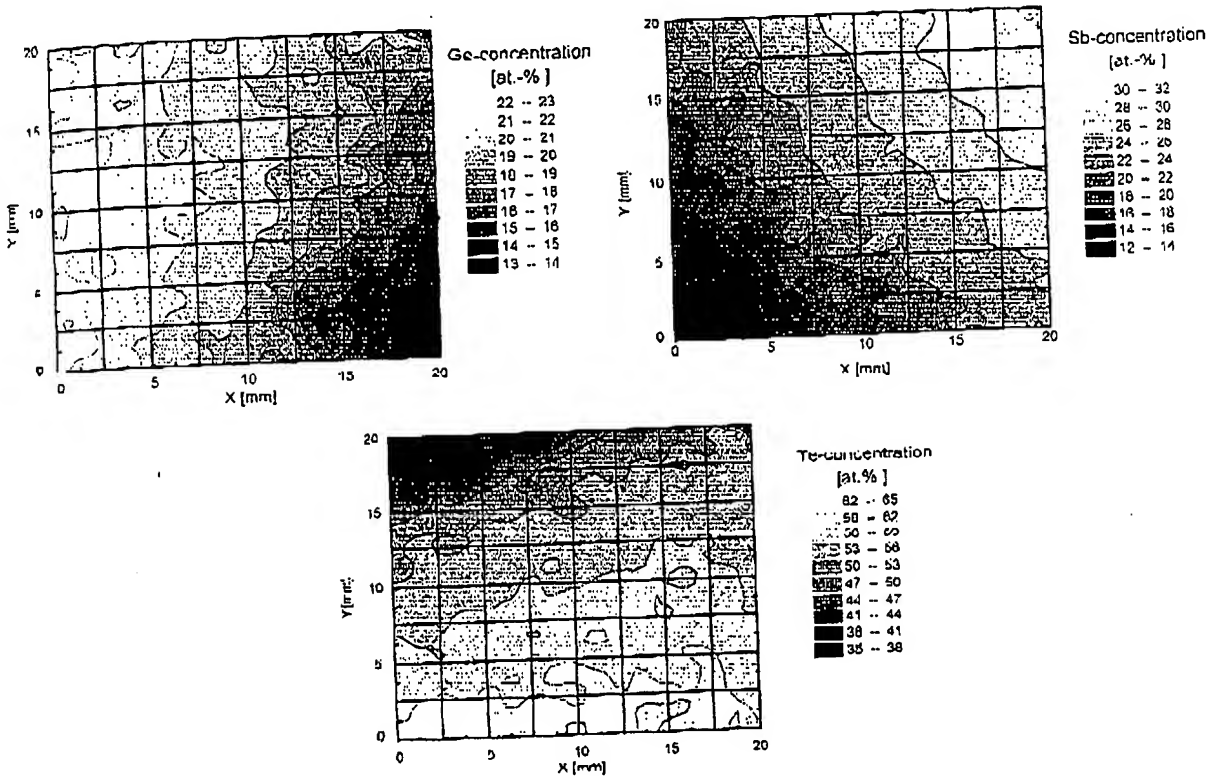

Fig. 13. EPMA mappings of the laterally graded Ge–Sb–Te film 1.

different distances from the gas inlet. Fig. 10 shows the diffractograms at four positions on the sample deposited at 480 V. Up to a distance of 115 mm from the gas inlet the deposited film remained single-phase cubic. Accordingly, the lattice parameter of the face-centered cubic unit cell almost linearly decreases with increasing Al content, thus corresponding to Vegard's law. Larger distances resulted in the formation of a two-phase mixture of cubic and hexagonal (Ti,Al)N.

The GIXRD analyses already indicated a strong influence of the substrate position on the film structure. Consequently, the morphology and the chemical composition of the coating deposited at a discharge voltage of 480 V were determined by SEM and EDX, respectively. The chemical composition of the deposited coating at different distances from the gas inlet is given in Table 2. The SEM images of cross-sections of the films deposited at distances of 41 and 151 mm are displayed in Fig. 11. In the upper right corner of each image, SEM images of the surface of the samples taken at the same magnification are inserted. The layer given in Fig. 11a has a columnar structure with grains extending from the interface to the surface, whereas the coating given in Fig. 11b has a rather fine-grained morphology. The growth of the crystallites was continuously interrupted by the nucleation of new grains. Obviously, the surface of this coating looks very similar to the morphology of the cross-sectional fracture. However, the surface morphology of the coating given in Fig. 11a appears much smoother.

The microhardness of all specimen was measured at different locations within the reaction chamber (Fig. 12). With increasing distance from the gas inlet and thus with increasing aluminum content incorporated in the coating the hardness increases. However, the dependence of the microhardness on the Al content is not linear, as the highest values are observed for coatings obtained near the cathode, exhibiting a two-phase structure of cubic and hexagonal

Table 3. Deposition parameters of the films. Films 1 and 2 were deposited on Si(111). Film 2 is a multilayer consisting of three sublayers a, b, and c.

Film no.	Deposition time [min]	$p(O_2)$ [Pa]	$p(Ar)$ [Pa]	P_{RF} [W]	P_{DC} [W]			
				Si	Al	Ge	Sb	Te
1	40	–	1	–	–	7.8	4.4	6.9
2a	5		0.6	–	200	–	–	–
2b	15	0.2	0.6	300	–	–	–	–
2c	5	–	1	–	–	7.7	4.4	6.8

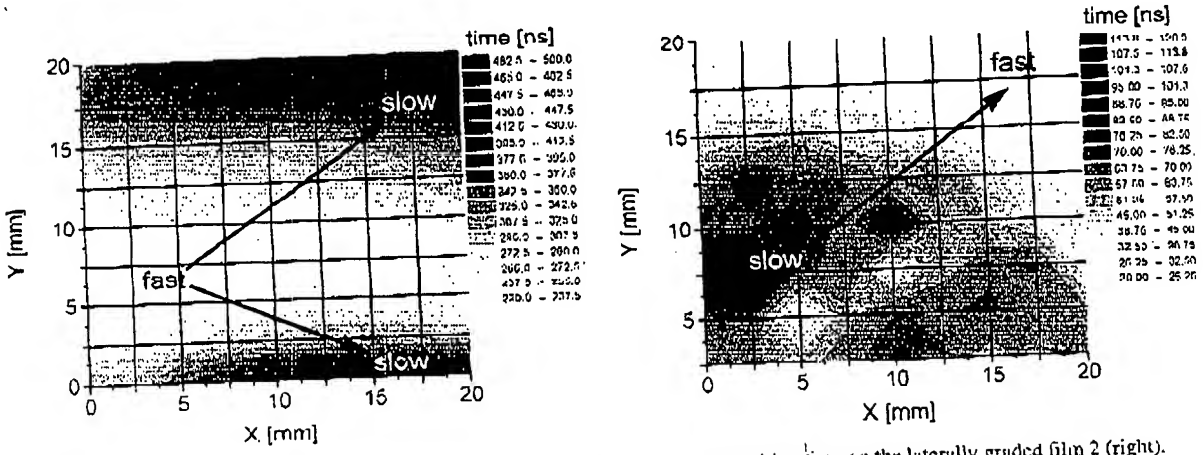

Fig. 14. Mapping of the crystallization time on the laterally graded film 1 (left) and writing time on the laterally graded film 2 (right).

(Ti,Al)N and thus showing the strong connection between microstructure and hardness. An influence of deposition parameters such as discharge voltage on the microhardness is not obvious.

5 Phase Change Velocity of Two-Dimensionally Graded Ge–Sb–Te Films for Rewritable Optical Data Storage

5.1 Experimental

Ge–Sb–Te films were deposited from separate Ge, Sb, and Te targets on Si(111) wafers and on Si(111)/Al/SiO_2 multilayers in a magnetron sputtering system in which the cathodes were arranged as shown in Fig. 3b. The residual gas pressure of the system is less than 10^{-5} Pa. The multilayers were deposited in a Leybold L560 reactive magnetron sputtering system prior to the deposition of Ge–Sb–Te. The deposition parameters of the films are summarized in Table 3.

EPMA elemental mappings and line-scans were carried out in a Camebax SX 50 microprobe. The laser induced phase change from amorphous to crystalline Ge–Sb–Te films was studied in a static tester. In this set-up, the phase change material is heated by a laser diode beam. Additional information on the experimental set-up can be found elsewhere [99Cre, 00Cre].

Depending on the laser power, the material is either transferred from amorphous to crystalline state, resulting in a change in reflectivity of about 20 %, or heated above the melting temperature and subsequently quenched back to the amorphous state. This transition from the crystalline to the amorphous phase is called the writing process, whereas the recrystallization is called the erasing process.

5.2 Results and Discussion

For quantitative analyses of the films EPMA element mappings were carried out. Fig. 13 shows the EPMA mapping of a Ge–Sb–Te film with a lateral compositional gradient of up to 30 at.% for each element around the ternary $Ge_2Sb_2Te_5$ phase, which is located near to the center of the wafer.

Fig. 14 (left) shows a mapping of the crystallization time of film 1. The mapping was performed in the same rectangular area of 20×20 mm^2 as given in the EPMA mappings. Using a laser power of 5.3 mW, the as-deposited amorphous phase changed to the crystalline phase. The area of fast transition, i.e., low crystallization time (white color), corresponds with a composition close to $Ge_2Sb_2Te_5$.

The writing process depends on a high cooling rate. Thus, a heat sink layer consisting of an aluminum film had to be integrated into the sample structure. A SiO_2 protection layer is also required to inhibit a contact of the Al film with Ge–Sb–Te. Fig. 14 (right) shows a mapping of the writing time of the laterally graded Ge–Sb–Te film 2 with an identical composition as film 1. Film 2 was deposited on a multilayer sample consisting of a Al/SiO_2 stacking on silicon. The mapping is the result of measurements in a rectangular area corresponding to the EPMA mapping in Fig. 13. Using a laser power of 9.3 mW, the film changed from the crystalline to the amorphous state. It was possible to affect a phase change on the whole sample. However, in the range of $Ge_2Sb_2Te_5$ the writing process is very slow caused by the fast crystallization process, as shown in Fig. 14. To avoid this influence a better heat sink would be sufficient.

The mappings of the crystallization time as well as of the writing time are plotted as a function of the corresponding composition in Fig. 15. Obviously, the crystallization time increased from 220 and 500 ns, depending on the composition, whereas the writing time was between 20 and 120 ns. The area with fast crystallization time and yet slow amorphization time corresponded with a composition of $Ge_2Sb_2Te_5$. With increasing distance from this chemical composition, the crystallization time increased at a simultaneous decrease in amorphization time.

6 Conclusions

These four different investigations have demonstrated the vast opportunities of combinatorial methods applied to materials development, thus leading to a minimum number of experiments that are necessary to obtain comprehensive results. A composition spread approach can easily be accomplished for magnetron sputtering through the adjustment of multiple cathodes. However, in this case combinatorial methods were also adopted for PECVD processes. Common to all four examples is the fact that certain materials properties, such as oxidation resistance, hardness or phase change velocity, can directly be correlated with the struc-

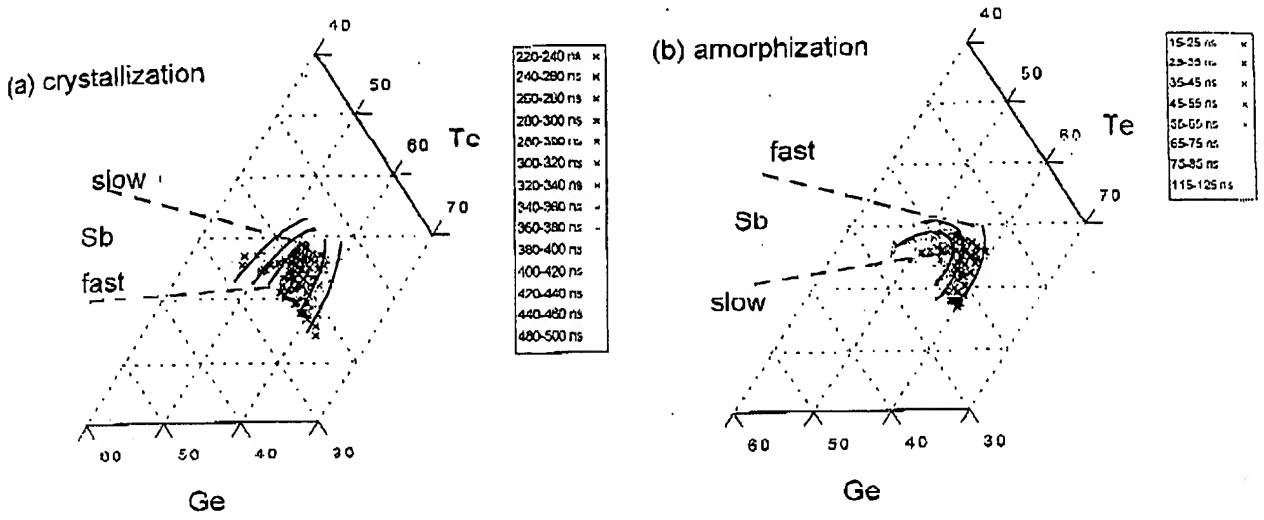

Fig. 15. Mapping of the crystallization time on the laterally graded film 1 (a) and writing time on the laterally graded film 2 (b) as a function of the film composition. Trend lines of both crystallization and amorphization times are inserted into the figures.

ture and composition of the deposited films. Therefore, the combinatorial approach appears to be a powerful and cost efficient tool for the development and optimization of new multicomponent functional materials.

The authors gratefully acknowledge the financial support granted by the Deutsche Forschungsgemeinschaft (DFG) within the Collaborative Research Center 289 and under contract no. Ne 351/22-1. In addition, the authors would like to thank the Institut für Halbleitertechnik II, RWTH Aachen, for the phase change measurements.

References

59Dar Darwin, C.: On the Origin of Species by Means of Natural Selection, or the Preservation of Favoured Races in the Struggle for Life, John Murray, London (1859).
69Saw Sawatzky, E.; Kay, E.: IBM J. Res. Develop. 13 (1969) 696.
70Han Hanak, J.J.: J. Mater. Sci. 5 (1970) 964.
97Cre Cremer, R.; Witthaut, M.; von Richthofen, A.; Neuschütz, D., in: I. Olefjord, L. Nyborg, D. Briggs (eds.), ECASIA 97, John Wiley & Sons, Chichester (1997) 963.
98Dov van Dover, R.B.; Schneemeyer, L.F.; Fleming, R.M.: Nature 392 (1998) 162.
99Cre Cremer, R.; Witthaut, M.; Neuschütz, D.; Trappe, C.; Facsko, S.; Kurz, H., in: P. Vincenzini (ed.), Ceramics: Getting into the 2000's, Part E, Techna Srl, Faenza (1999) 501.
99Jan Jandeleit, B.; Schaefer, D.J.; Powers, T.S.; Turner, H.W.; Weinberg, W.H.: Angew. Chem. Int. Ed. 38 (1999) 2494.
99Pra Prange, R.; Neuschütz, D.: J. Phys. IV 9 (1999) Pr8-811.
00Cre Cremer, R.; Witthaut, M.; Neuschütz, D.; Trappe, C.; Laurenzis, M.; Winkler, O.; Kurz, H.: Mikrochim. Acta 133 (2000) 299.
01Kyr Kyrsta, S.; Cremer, R.; Neuschütz, D.; Laurenzis, M.; Haring, P.; Kurz, H.: Appl. Surf. Sci. 179 (2001) 55.

(Received April 28, 2001)

Correspondence Address

Dr. R. Cremer
Lehrstuhl für Theoretische Hüttenkunde, RWTH Aachen
D-52056 Aachen, Germany
Fax: +49 241 80 22 295
E-mail: Cremer@LTH.RWTH-Aachen.de